3-D Printed Planar Dielectric Linear-to-Circular Polarization Conversion and Beam Shaping Lenses Using Coding Polarizer

Jianfeng Zhu, *Student Member, IEEE*, Yang Yang, *Senior Member, IEEE*, David McGloin, Ranjith Rajasekharan Unnithan, *Member IEEE*, Shaowei Liao, *Senior Member, IEEE,* and Quan Xue, *Fellow, IEEE*

Abstract—**This paper presents a new linear-to-circular polarization (CP) conversion coding unit, on which two new kinds of beam shaping lenses are proposed. Firstly, under periodic boundary conditions, a linear-to-circular polarization conversion coding unit is introduced, which introduces the necessary phase delay by adjusting its geometrical parameters. The phase delay ranges from 0 to 360° and is discretized into 3-bit coding units corresponding to specific delays. Secondly, by properly arranging the coding units, a high gain CP lens is proposed. The lens achieves linear to circular polarization conversion and beam collimation in the transmission mode simultaneously with a planar configuration, which is different from counterparts that place a lens atop of a polarizer. Furthermore, the coding units are used to form Wollaston-prism-like and Rochon-prism-like planar CP beam shaping lenses, which split the beams with different polarizations into right and left-handed components. These beams can be controlled independently. Prototypes working at 30-GHz band are designed, fabricated and measured to verify the idea.**

***Index Terms*—3D printing, millimeter-wave (mm-Wave), lens, beam shaping, coding polarizer, pencil-beam.**

I. Introduction

Recently, beam shaping and polarization manipulation of electromagnetic (EM) wave have drawn considerable attention with remarkable achievements. With the rise of the metamaterial, many interesting and exciting devices that are capable of focusing light [1-3] steering beam [4-6] or generating orbital angular momentum [7-9] have been proposed from optics to microwave. As for the polarization manipulation, circular polarizers that convert the linearly polarized (LP) waves into circularly polarized (CP) ones are commonly used. Quarter-wave plates (QWPs) are well-known circular polarizers that are widely used in optics [10]. They can be realized by exploiting the inherent birefringence in natural materials, such as crystalline quartz [11], or by inducing birefringence grating structures [12], [13]. At microwave/millimeter-wave (mm-wave) frequencies, many circular polarizers have been reported [12-18]. They can be categorized into metal and dielectric-based devices. For metal-based circular polarizer, they can be implemented by using meander-line [14-16] or frequency selective surfaces [17]. For example, a Ka-band polarization converter was proposed over a wide frequency band from 23 to 35GHz (42%) by using metallic circular traces printed periodically on each dielectric multilayer slab [18]. For dielectric-based ones, dielectric gratings can create birefringence for two orthogonal polarizations, which is a common approach to form a CP polarizer [19-21].

In the mm-wave band, QWP-based lenses combining polarization conversion and beam shaping are particularly desirable. This is because the high directivity of the lens can compensate the high path loss at mm-wave frequencies [22] and a CP antenna is capable of preventing performance degradation caused by the misalignment between the transmitting and receiving antennas [23], [24]. Many lens antennas with a CP source have been proposed [25-33]. Recently, a broadband circularly polarized antenna using an artificial anisotropic polarizer operating in the 60-GHz frequency band was proposed [25]; a hyperbolic lens was used to collimate the beams, and an artificial anisotropic polarizer was used to convert LP to CP. Wang. et.al [31] proposed a circularly polarized antenna using a dielectric polarizer. With the help of the polarizer, the directivity of the radiation pattern is also enhanced. Then, a CP lens antenna with LP feeding was also proposed [32], which is formed by a cylindrical polarizer stacked with a hemispherical dielectric lens. The cylindrical polarizer, composed of dielectric grating and air slabs, can convert the incident wave from LP into CP and a hemispherical dielectric lens is used to improve the antenna gain. Later on, Wu. et.al [33] demonstrated a terahertz CP lens antenna, where the transmit-array is used to replace the conventional lens. Though these CP lenses show wide CP bandwidth and high gain, they are implemented by geometrically placing a lens or transmit-array above a quarter-wave phase plate. Moreover, traditional lenses [32] and dielectric transmit-arrays with different unit-cell heights [33] make the design non-planar. Therefore, a geometrically planar and compact lens with both CP conversion and beam collimation/shaping is highly desired for mm-wave applications.

Metamaterials, often engineered by judiciously placing artificial structures with tailored meta-atoms at subwavelength

Manuscript received XX, 2019. This work was supported partly by the National Science Foundation of China under Grant 61871189, and Science Foundation of Guangdong Province under Grant 2019A1515011999, and the Fundamental Research Funds for the Central Universities under Grant 2018MS14, and the Guangdong Innovative and Entrepreneurial Research Team Program (No. 2017ZT07X032). (Corresponding author: Shaowei Liao)

Jianfeng Zhu is the School of Electronic and Information Engineering, South China University of Technology, Guangzhou 510006, China, with school of Electrical and Data Engineering, University of Technology Sydney, Ultimo, NSW 2007, Australia. and also with Beijing Key Laboratory of Network System Architecture and Convergence, Beijing University of Posts and Telecommunications, Beijing 100876, China, (e-mail: jianfeng.zhu@uts.edu.au).

Yang Yang and David McGloin are with school of Electrical and Data Engineering, University of Technology Sydney, Ultimo, NSW 2007, Australia (e-mail: yang.yang.au@ieee.org, david.mcgloin@uts.edu.au)

Ranjith Unnithan is with Department of Electrical and Electronic Engineering, The University of Melbourne, (email: r.ranjith@unimelb.edu.au).

Shaowei Liao and Quan Xue are with the School of Electronic and Information Engineering, South China University of Technology, Guangzhou 510006, China, (e-mail: liaoshaowei@scut.edu.cn eeqxue@scut.edu.cn).

TABLE I. THE DESIGNED 3-BIT CODING UNITS USING DIFFERENT SCALE OF QWP

3-bit coding	000	001	010	011	100	101	110	111
Phase response	0°	45°	90°	135°	180°	225°	270°	315°
Geometry (*w,l*) (mm)	(1.4,7.4)	(2.25,6.2)	(2.7,6.4)	(3.1,6.8)	(3.45,7.1)	(3.8,7.5)	(4.1,7.8)	(4.5,8)

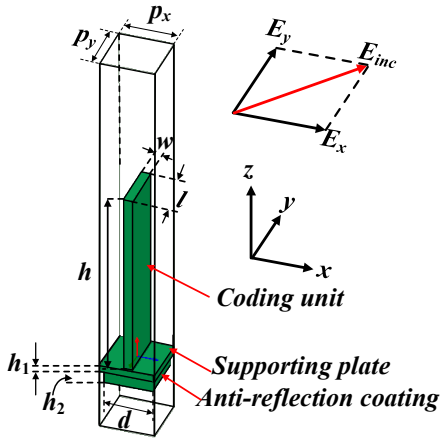

Fig.1. Configurations of the proposed coding unit cells. (P_x=8 mm, P_y=8 mm, h=28mm, h_1=1 mm, h_2=1.9 mm, d=7.2 mm)

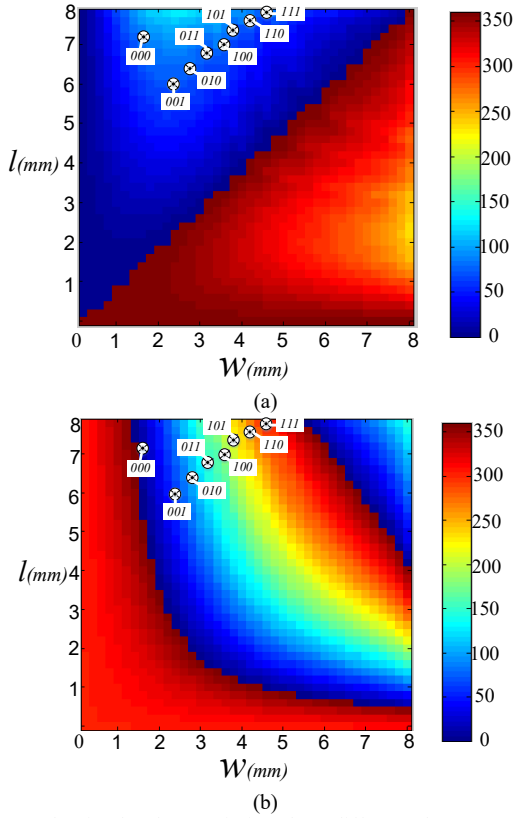

Fig. 2. (a) The simulated transmission phase difference between x-pol and y-pol incident waves as a function of (w, l) at 30-GHz. (b) The simulated transmission phase as a function of (w, l) at 30-GHz.

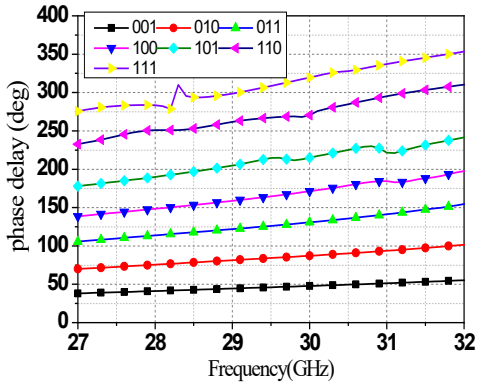

Fig.3. Transmission phase delay of the 3-bit coding unit cells (compared with 000 unit).

scales to control electromagnetic waves, possess properties that are not normally found naturally [34]. Taking advantage of metamaterials, many planar lenses with high directivity and aperture efficiency have been proposed [35-37]. Usually, metamaterials are described by effective medium parameters (e.g. index of refraction, permittivity and permeability) due to the subwavelength nature of meta-atoms [38]. Recently, the use of coding metamaterials has been suggested for the control of electromagnetic waves through the design of coding sequences using digital elements '0' and '1,' which possess opposite phase responses [39]. The concept of coding metamaterials can be extended from 1-bit coding to 2-bit coding or even higher to manipulate EM waves in different manners by properly programming different coding sequences [40].

In this paper, a new linear-to-circular polarization conversion coding unit with a basic structure shown in Fig. 1 is proposed. Under periodic boundary conditions, by adjusting the unit width (w) and length (l) of the array with a fixed height (h), the LP E-field vector can be converted to CP with a phase delay ranging from 0 to 360°. The phase is discretized into 3-bit groups, namely, 0°, 45°, 90°, 135°, 180°, 225°, 270°, and 315° (corresponding to the "000", "001", "010", "011", "100", "101", "110", and "111" coding). Then, based on the coding unit, a CP lens with high gain pencil beam is proposed. Compared with its counterparts that place a lens atop of a polarizer, our CP lens enjoys the benefit of merging linear to circular polarization conversion and beam collimation in a single component with a planar configuration and reduced thickness. Furthermore, based on the same coding unit, we propose Wollaston-prism-like and Rochon-prism-like planar CP beam shaping lenses. These lenses split the beam into orthogonal circularly polarizations and the two beams can be controlled independently. Prototypes of the lenses are designed, fabricated and measured to verify the idea.

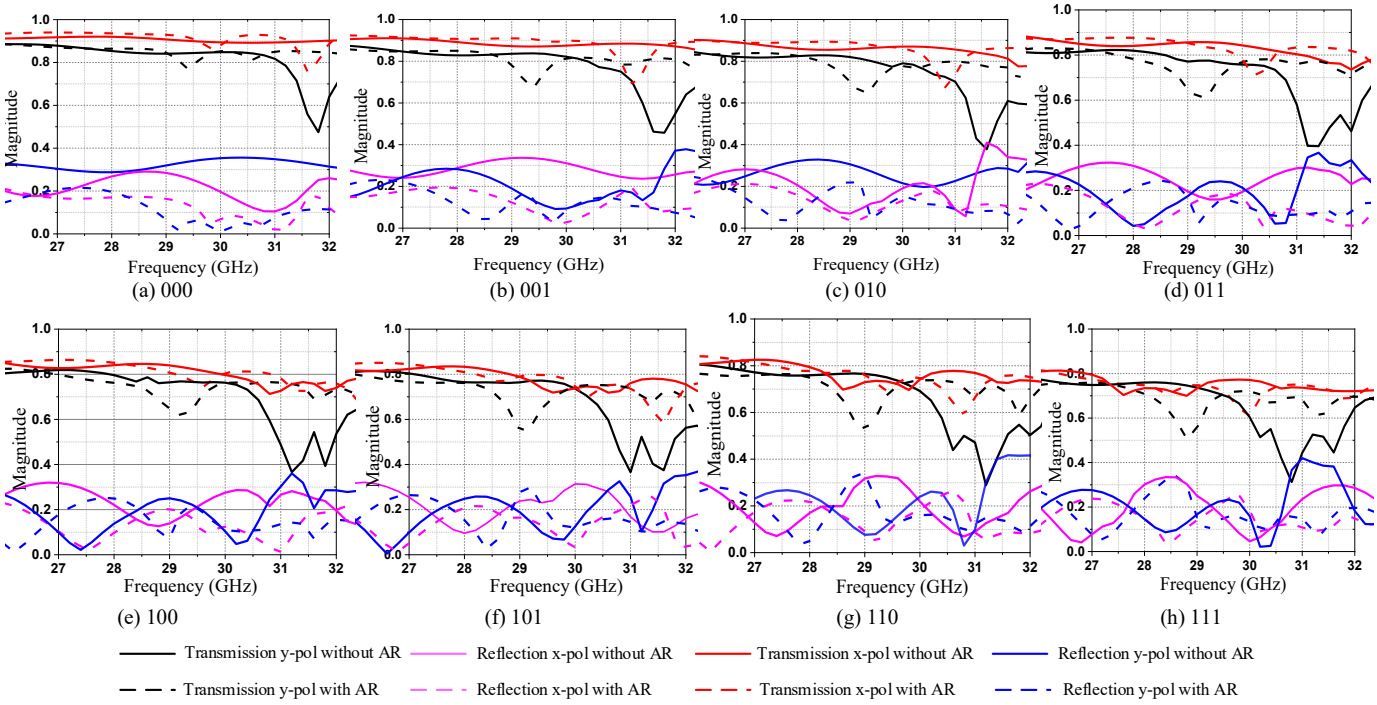

Fig. 4. Transmission and reflection magnitudes of the eight coding units with and without AR coating.

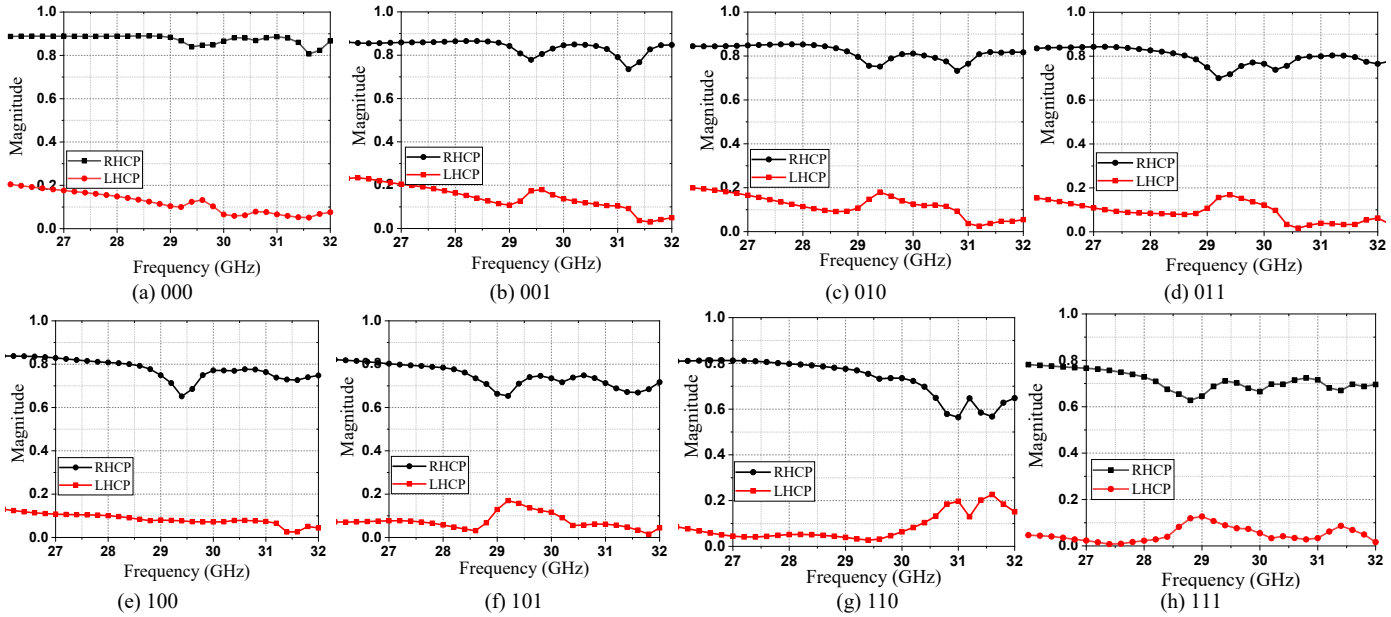

Fig. 5. Magnitudes of the transmitted RHCP and LHCP of eight coding units.

II. 3-Bit Coding Polarizer Units Design

The basic geometry of the coding unit cell is shown in Fig. 1 (a), which is simulated and optimized in ANSYS HFSS. The cell is composed of a coding unit, a supporting plate and an anti-reflection (AR) coating, which are stacked in order. Polylactic acid (PLA) with a relative dielectric constant 2.5 and loss tangent of about 0.02 at 30-GHz is used in the design. To reduce the impact of fabrication tolerance, we choose a period of 0.8-wavelength at 30-GHz for proof-of-concept. In the simulation, periodic boundary conditions (PBCs) are set along the x and y-directions and Floquet ports are used as the excitation. Since the unit is designed with periodic boundaries, it is equal to a unit in an array with infinite uniform units. This means the performance (LP-to-CP conversion and phase delay) of each unit in the lens is different from those of the corresponding unit in an array with infinite uniform units, because of the change of the boundaries. The performance differences are small and acceptable for lens design. This is because the units forming the lens slowly change to form the lens, namely two adjacent units are very similar in structure, which leads similar boundaries for units in a lens and in an array with infinite uniform units.

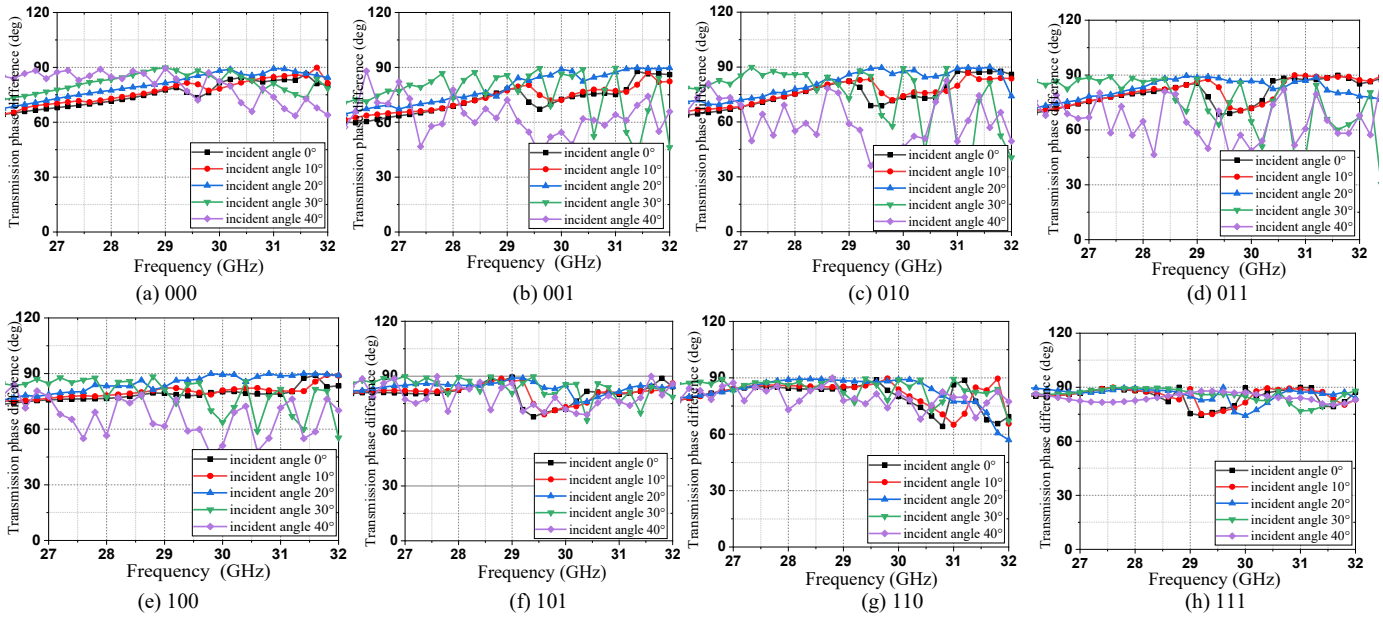

Fig. 6. Transmission phase difference of the TE and TM modes at different incident angles of the eight coding units.

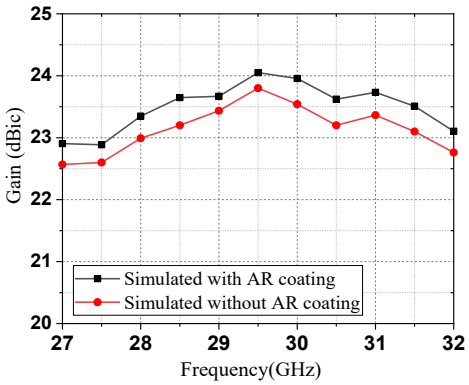

Fig.7. Simulated lens peak gains with and without the AR coating.

The incident electric field passing through the polarizer is decomposed into two orthogonal components, E_x and E_y, as shown in Fig. 1. Since the unit cell is anisotropic along with x and y- directions, E_x and E_y propagate through it with different phase velocities. By adjusting the geometric values (w,l) of the polarizer, the required 90° phase difference between E_x and E_y can be realized, which results in a CP wave. Different from conventional circular polarizers [31-33] using uniform QWP cells, the proposed 3-bit coding QWP cells exhibit different transmission phase. Namely, different geometric values (w, l) can realize 90° phase difference between E_x and E_y but with different overall unit cell transmission phases. Therefore, by properly choosing the geometric values (w, l), the QWP cells can have the same amplitude of transmission coefficient but with eight phase delays of 0°, 45°, 90°, 135°, 180°, 225°, 270°, and 315°, corresponding to the "000", "001", "010", "011", "100", "101", "110", and "111" coding. In order to provide 360° transmission phase delay and minimize the thickness, the height of all the coding cells is adopted as 28mm. Therefore, only the length and width of the unit cells are optimized. The 3-bit coding units (w, l) should satisfy two conditions: (1) Each coding unit should provide 90-degree phase difference between x-pol and y-pol incident waves. (2) Eight unit cells should provide the 0 to 2π full transmission phase circle. Therefore, our design strategy is: first, we obtain two phase masks, namely, a transmission phase difference between x-pol and y-pol incident waves as a function of (w, l) and a transmission phase as a function of (w, l), as shown in Figs. 2 (a) and (b), respectively. Then, according to Fig. 2 (a), we can locate the region that we are interested in, i.e. phase difference around 90-degree. Then, in the same region in Fig. 2 (b), we can select the 3-bit coding units that provide the 0 to 2π full transmission phase circle. It is also worth mentioning that, as seen from Fig. 2, the proposed coding units are not a unique solution. The designed 3-bit coding sequence is shown in Table I. Their transmission phase delay curves versus frequency are shown in Fig. 3. The transmission magnitudes of the x-pol and y-pol incident waves and the transmission magnitudes of the RHCP and LHCP (cross-pol) conversion of the eight coding units are given in Figs 4 and 5, respectively. It is seen that the transmission loss is gradually increased with the codes due to the relatively high dielectric loss of the printing material. Fig. 6 shows the transmission phase difference of the TE and TM modes of the eight unit cells under different incidence angles from normal to 40-degrees. It is observed that the performance of the cells is insensitive up to 20-degrees.

To reduce the strong reflection at the interface between the air and dielectric supporting plate, an AR coating is added below the supporting plate. The AR coating is realized using a square plate, the thickness (h_2) and permittivity (ε_{AR}) of the AR structure required for zero reflectivity are [41]:

$$h = \frac{\lambda_{AR}}{4} \qquad \text{and} \quad \varepsilon_{AR} = \sqrt{\varepsilon_{air}\varepsilon_{PLA}} \tag{1}$$

where λ_{AR} is the wavelength in the AR structure, ε_{air} and ε_{PLA} are the dielectric constant of air and PLA, respectively. Therefore, $\varepsilon_{AR} \approx 1.58$, and $h \approx 2.0$ mm. In the design,

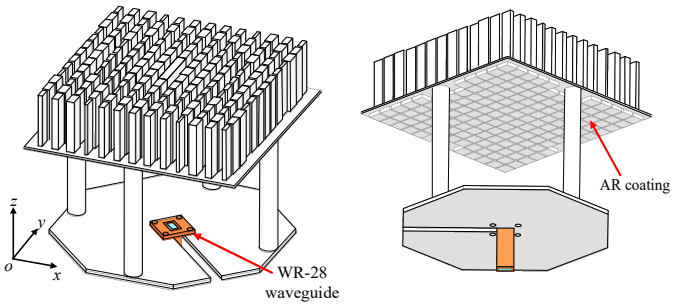

Fig.8. The configurations of the CP-lens with WR-28 waveguide feed.

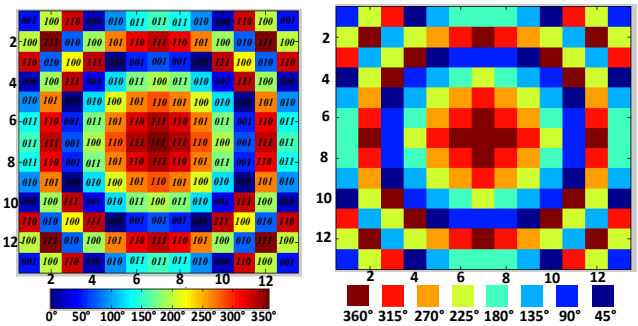

Fig. 9. (a) Compensating phase at the lens aperture and the corresponding code. (b) The discretized phase distribution at the aperture using coding unit cell.

considering that there are reflections at the boundary between air/supporting plate, supporting plate/polarizer and polarizer/air, the thickness and the length of the AR coating is optimized with the goal of minimizing reflection of the unit. The final optimized size of the AR coating is 7.2×7.2×1.9 mm^3.

The transmission and reflection magnitudes of the eight coding units with and without AR coating are shown in Fig. 4 for comparison. It is seen that by using the AR coating, the reflection magnitude can be improved, especially for the 000, 001, 010 and 011 units, and the transmission magnitudes are significantly improved above 30-GHz. Adding the AR coating introduces a transmission minimum point at about 29-GHz for the y-polarized incident wave. Nevertheless, according to the transmitted magnitude of the RHCP shown in Fig. 5 and the gain comparisons with/without AR coating of the lens shown in Fig. 7, after adding the AR coating, the RHCP gain of the lens does not show much of a drop at this point but the average gain improves by 0.4-0.5 dB.

III. CP Lens Antenna Design

A. Lens Antenna Configuration

Based on the proposed 3-bit coding unit cells, a planar QWP lens with 169 (13×13) cells in a square aperture operating at 30-GHz is designed. The configuration of the proposed QWP-lens is shown in Fig. 8. A WR-28 waveguide feed the lens and is arranged 45 ° with respect to the *ox*-axis. Because the CP lens is designed based on the phase curves under the normal incidence for simplicity, using a relatively large focal to diameter (F/D) ratio can reduce the effects of incident angle on the lens performance. Also considering the tradeoff between the illumination efficiency and spillover efficiency, the F/D is adopted as about 0.81. The desired phase compensation at each unit cell is obtained according to Fermat's principle of equality

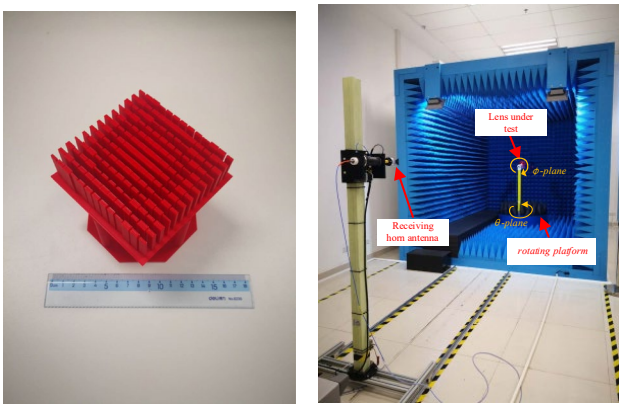

Fig.10. (a) Lens prototype. (b) Mm-wave far-field measurement system.

of electrical path lengths of incoming electromagnetic waves [42]:

$$\varphi(x,y)=\frac{2\pi}{\lambda_0}\left(\sqrt{x^2+y^2+f^2}-f\right)+\varphi_0 \qquad (2)$$

where f represents the focal length, λ_0 represents wavelength in free space, φ_0 represents the initial phase at the original point. The obtained compensating phase at the lens aperture is shown in Fig. 9 (a) and then it is discretized by using the coding unit cells, as shown in Fig. 9 (b). The phase center of the feed at 30-GHz is initially placed at the focal point of the lens. Then, considering the thickness of the lens and the phase center is varying with frequency and direction, the position of the feed along z-direction is slightly optimized to obtain the highest and stablest gain within the entire frequency band.

B. Fabrication and Measurement

The designed lens is fabricated using a commercial Raise3d Pro2 printer. The fabricated lens prototype is shown in Fig. 10 (a). The lens is measured using a far-field mm-wave antenna measurement system, as shown in Fig. 10 (b). The measured 3-D radiation patterns and the 2-D simulated and measured radiation patterns at 27, 28, 29, 30-GHz are shown in Fig. 11 (a), (b) and (c), respectively. The simulated and measured results agree well. A Pencil-beam with high directivity can be observed and the sidelobe level of the beams are kept well below -15 dB. The simulated and measured RHCP gains and the axial ratio of the lens are shown in Fig. 12. The 3-dB axial ratio bandwidth is from 25 to >33-GHz. The RHCP gains are from 22.8 to 24 dBic for the simulation and from 21.5 to 22.6 dBic for the measurement from 28 to 32-GHz.

IV. Beam Splitting Lens Design

we extended the coding unit cells to form a Wollaston-prism-like and Rochon-prism-like planar circularly polarized beam shaping lenses. A Wollaston prism and Rochon prism split the beam into two beams with perpendicular polarizations. The split beams leave the Wollaston prism at a symmetrical divergence angle (Figure 13 (a)), while the Rochon prism (Figure 13 (b)) refracts only the extraordinary (ordinary) wave but allows the ordinary (extraordinary) wave to propagate undeviated. However, conventional polarization beam splitters are based on by naturally anisotropic materials, which require a

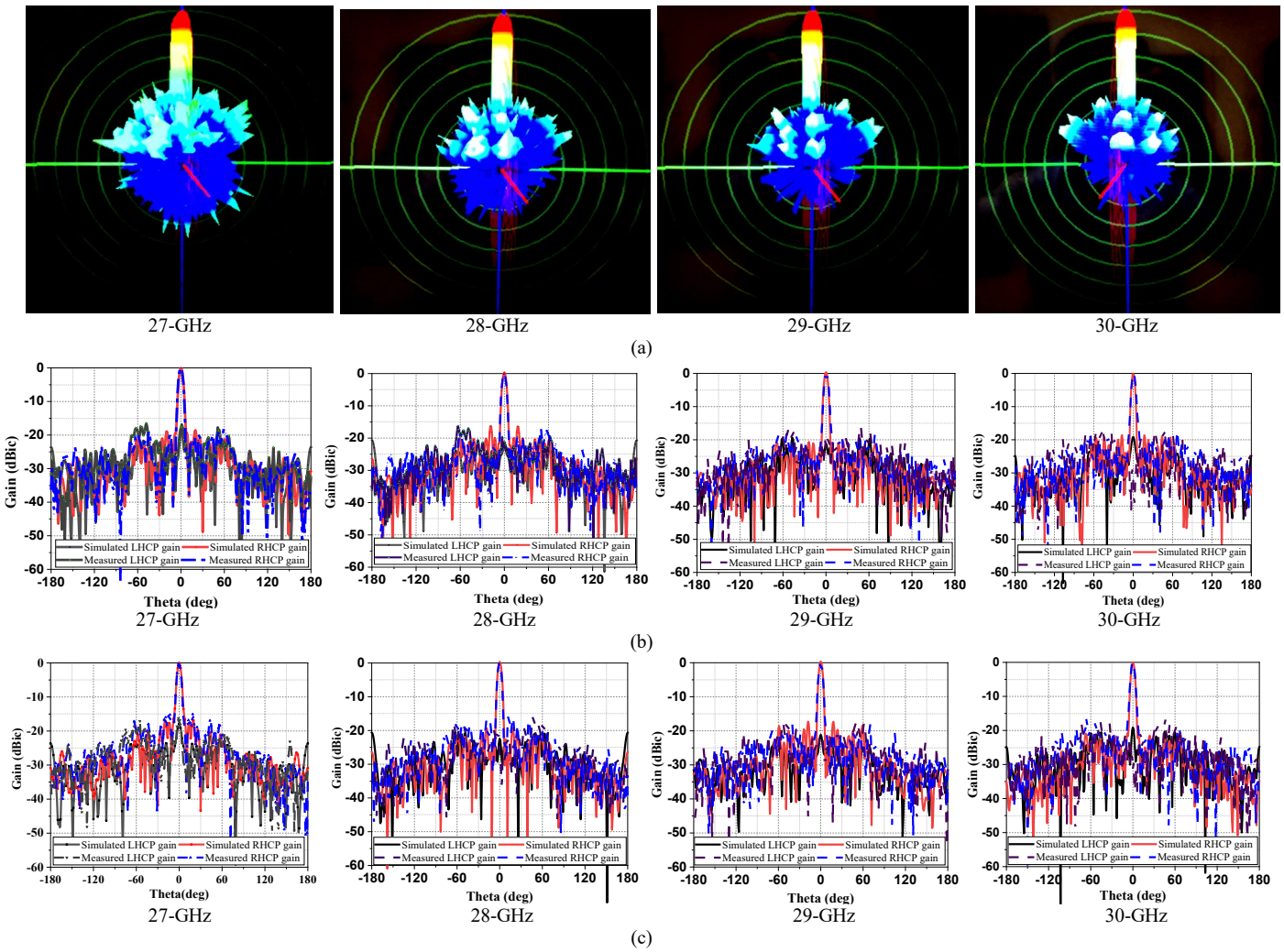

Fig. 11. (a) Measured 3D RHCP radiation patterns: pencil beams. (b) Simulated and measured radiation patterns at xoz-plane. (c) Simulated and measured radiation patterns at yoz-plane.

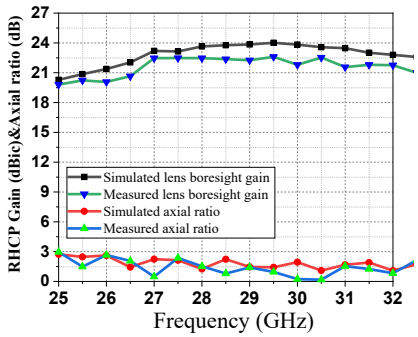

Fig. 12. Simulated and measured RHCP gain and axial ratio.

large thickness to generate enough walk-off distance between the two orthogonal polarizations owing to the intrinsically small birefringence [10]. Moreover, for practical optical systems, an additional lens has to be put in front of the prisms to collimate the beams, which makes the system complicated and bulky. The proposed beam splitting lens, on the other hand, collimates the beams and manipulates the orthogonal polarizations simultaneously with a low-profile planar form. This can significantly ease these burdens aforementioned, as shown in Fig. 13 (c) and (d).

A. Wollaston-Prism-Like Planar Circularly Polarized Beam Shaping Lens Design.

The configurations of the proposed Wollaston-prism-like circularly polarized beam shaping lens is shown in Fig. 14 (a). The unit cells used here are the same as that used in Section II. 14×14 coding unit cells are adopted in the design. The orientation of the unit cells in the left half part of the lens are arranged orthogonally to that in the right part to generate two orthogonal circularly polarization beams with equal power. To split the beam for the two circular polarizations, an additional phase φ_{xn} is added to the compensating phase of the lens on each column along the x-direction, where φ_{x1}=0°, φ_{x2}=-45°, φ_{x3}=-90°, φ_{x4}=-135°, φ_{x5}=-180°, φ_{x6}=-225°, φ_{x7}=-270°, φ_{x8}=-270°, φ_{x9}=-225°, φ_{x10}=-180°, φ_{x11}=-135°, φ_{x12}=-90°. φ_{x13}=-45°, φ_{x14}=-0°. The compensating phase at the lens aperture, shown in Fig. 15 (a), is discretized by the coding unit cells, as shown in Fig. 15 (b). For normal incidence, the angle of the tilted beam can be calculated as [44]:

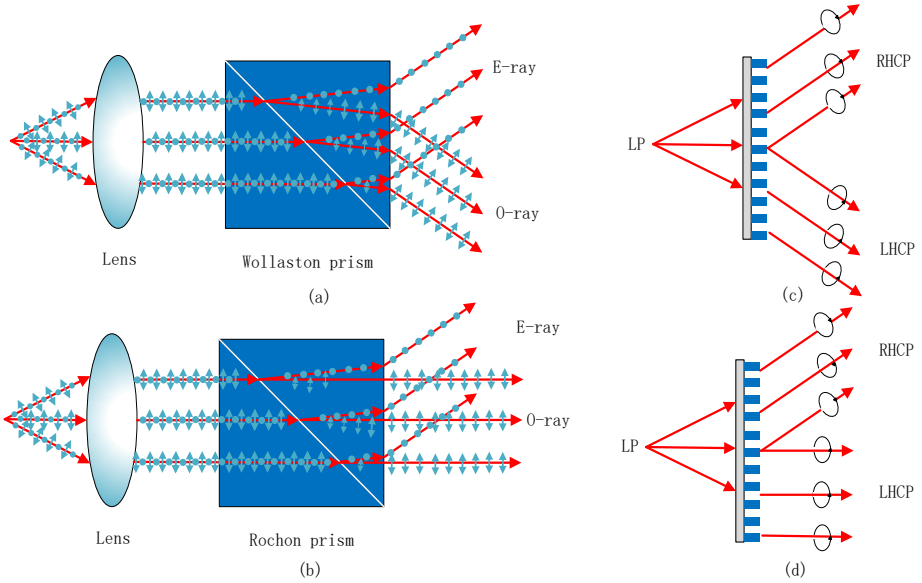

Fig. 13. (a) Wollaston prism that deflects the collimated extraordinary and ordinary rays. (b) Rochon prism that only deflects the collimated extraordinary ray. (c) Proposed design that collimates and symmetrically deflects both RHCP and LHCP rays. (d) Proposed design that collimates rays and only deflects the RHCP rays. (The extraordinary wave corresponds to the case of the electric field polarized perpendicular to the plane of incidence. The ordinary wave corresponds to the case of the magnetic field polarized perpendicular to the plane of incidence [41]).

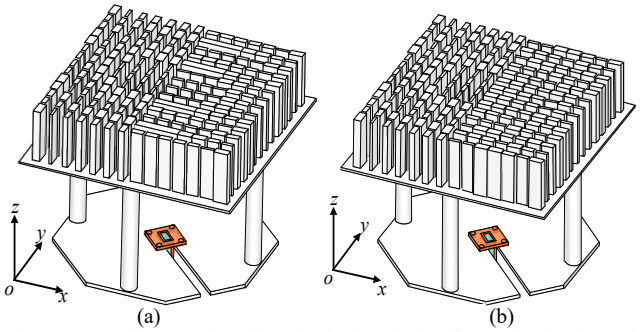

Fig. 14. (a)Wollaston-prism-like circularly polarized beam shaping lens. (b) Rochon-prism-like circularly polarized beam shaping lens.

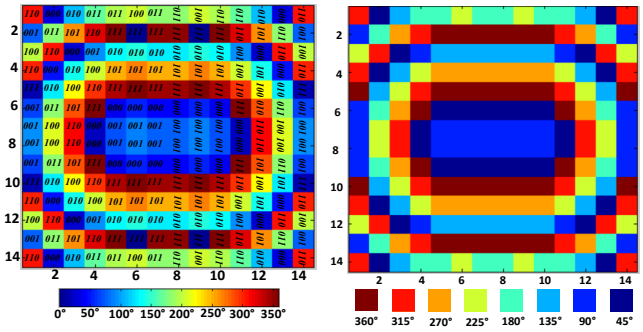

Fig. 15. (a) Compensating phase at the lens aperture and the corresponding code. (b) The discretized phase distribution at the aperture after using coding unit cell.

$$\theta=\sin^{-1}\frac{\lambda}{2\pi}\frac{d\varphi}{dx} \qquad (4)$$

where $d\varphi/dx$ is the phase gradient along the ox-direction. The simulated and measured lens radiation patterns at 28, 30-GHz and 32-GHz are shown in Fig. 16. It is seen that LHCP and RHCP are symmetrically split with a deflecting angle of 9.2-degrees (28-GHz), 10-degrees (30-GHz) and 10.2-degrees (32-GHz). The maximum angular deviation is less than 1-degree compared to the central frequency (30-GHz). The simulated and measured peak RHCP/LHCP gains, as well as the lens prototype, are shown in Fig. 17. The simulated peak gains span from 16.2 to 18 dBic and measured peak gains range from 15.8 to 16.9 dBic over the operating band.

B. Rochon-Prism-Like Planar Circularly Polarized Beam Shaping Lens Design.

The configurations of the proposed Rochon-prism-like circularly polarized beam shaping lens is shown in Fig. 14 (b). Similar to the Wollaston-prism-like lens, it consists of 14×14 unit cells with the orientation in the left half part arranged orthogonal to that in the right part. In order to refract only one circularly polarization while allows the other circularly polarization to propagate undeviated, additional phases that are added to the compensating phase of the lens on each column along x-direction are φ_{x1}=0°, φ_{x2}=-45°, φ_{x3}=-90°, φ_{x4}=-135°, φ_{x5}=-180°, φ_{x6}=-225°, φ_{x7}=-270°, φ_{x8}=0°, φ_{x9}=0°, φ_{x10}=0°, φ_{x11}=0°, φ_{x12}=0°, φ_{x13}=0°, φ_{x14}=0°. Then, the compensating phase, shown in Fig. 18 (a) is discretized by the coding unit cells, Fig. 18 (b). The normalized simulated and measured lens radiation patterns at 28, 30-GHz and 32-GHz are shown in Fig. 19. The RHCP beam is tilted with an angle of 9.6-degrees (28-GHz), 10.8-degrees (30-GHz) and 11-degrees (32-GHz). The simulated and measured peak RHCP/LHCP gains, as well as the lens prototype, are shown in Fig. 20. The simulated peak gains range from 17.3 to 17.8 dBic for RHCP and from 16.1 to 16.4 dBic for LHCP. The measured gains span from 15.3 to 16.4 dBic for RHCP and from 15.2 to 15.7 dBic for LHCP from 28 to 32 GHz. The beam splitting lenses are not limited dual beam with different circular polarizations. It can be extended to one beam of circular polarization and the other beam with linear polarization by planting half of the cells with coding QWP and the other half with coding half-wave plate (HWP).

TABLE II
COMPARISON OF DIFFERENT CIRCULARLY POLARIZED LENS ANTENNA

Ref.	Antenna Type	Shape	Fabrication technique	Thickness (mm)	Working bands (GHz)	3dB AR bandwidth	Peak Gain (dBic)	Remarks
[26]	Helics source +lens	Non-planar	3-D inkjet-printing	69 (3.2 λg)	8.8-GHz	5.5%	16.4	High aperture efficiency, medium AR bandwidth, medium gain, CP source
[27]	CP patch source +lens	Non-planar	PCB+ machining technique	0.508 (0.08 λg)	28-GHz	Not given	18.5	High aperture efficiency, medium gain, CP source
[28]	CP patch source +lens	Non-planar	PCB+ machining technique	7 (1.05 λg)	30-GHz	4%	13.4	Medium aperture efficiency, medium AR bandwidth and gain, CP source
[29]	CP patch source +lens	Non-planar	PCB+ machining technique	81.908 (12.8 λg)	30-GHz	2.6%	25.9 (directivity)	High aperture efficiency, medium AR bandwidth, high gain, CP source
[30]	CP leaky wave source +lens	Non-planar	PCB+ machining technique	N.A.	180-GHz	35%	35.8	Beam steering, high aperture efficiency, wide AR bandwidth, high gain, LP source
[32]	CP lens	Non-planar	3-D printing	16.5 (5.61 λg)	60-GHz	29%	21.4	High aperture efficiency, wide AR bandwidth, high gain, LP source
[33]	CP lens	Non-planar	3-D printing	4.2 (6.85 λg)	300-GHz	18.8%	30.8	High aperture efficiency, wide AR bandwidth, high gain, LP source
[45]	CP transmitarray	Planar	PCB	1.13 (0.19 λg)	30-GHz	24.2%	22..8	High aperture efficiency, wide AR bandwidth, high gain, LP source
[46]	CP transmitarray	Planar	PCB	1 (0.12 λg)	10-GHz	3.5%	21.9	High aperture efficiency, wide AR bandwidth, high gain, LP source
[47]	CP transmitarray	Planar	PCB	12.7 mm (0.59 λg)	14-GHz	12.6%	24.5	High aperture efficiency, wide AR bandwidth, high gain, LP source
This work	CP lens	Planar	3-D printing	30.9 mm (4.88 λg)	30-GHz	>27%	22.6	Wide AR bandwidth, high gain, LP source

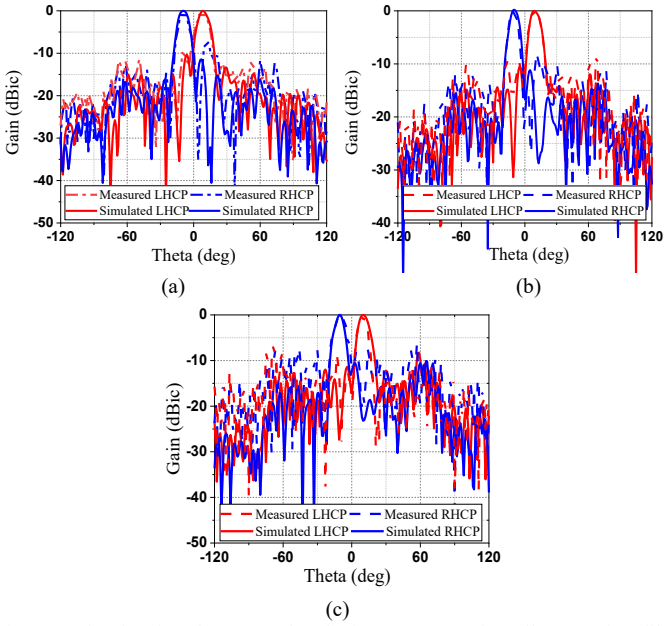

Fig. 16. Simulated and measured radiation patterns of Wollaston-prism-like circularly polarized beam shaping lens at (a) 28-GHz, (b) 30-GHz and (c) 32-GHz.

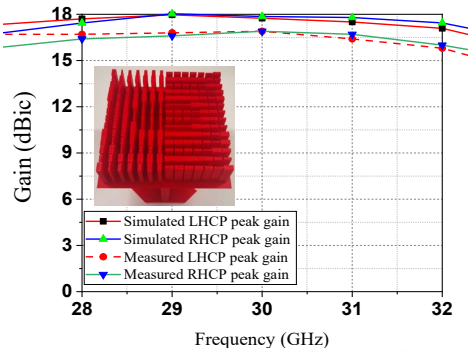

Fig. 17. Simulated and measured peak gain of Wollaston-prism-like circularly polarized beam shaping lens (The inset shows the printed prototype).

V. COMPARISONS AND DISCUSSION

Table II compares the proposed work with other circularly polarized lens antennas. Integrating a lens with a circularly polarized source is a common approach to achieve high gain CP antenna. The CP source can be a conventional circularly polarized helix antenna [26] or patch [27-29]. However, the CP source increases the design complexity and the patch-based CP antennas usually suffer from narrow impedance and AR

TABLE III
COMPARISON OF DIFFERENT POLARIZATION-DEPENDENT BEAM SPLITTING DESIGN

Ref.	Antenna Type	Fabrication technique	Thickness	Working band	Beam splitting Principle	Remarks
[5]	LP beam splitting	PCB	3mm (0.16 λg)	10-GHz	anisotropic gradient-index metamaterials	Large deflecting angle, splitting angles independent tuning
[48]	LP beam splitting	PCB	25.6 mm (1.42 λg)	10-GHz	anisotropic gradient-index metamaterials	Large deflecting angle, splitting angles independent tuning, lens
[49]	CP beam splitting	PCB	1.9mm (0.13 λg)	10-GHz	PB phase	Large deflecting angle, Symmetrical splitting angle.
[50]	CP beam splitting	PCB	9mm (0.13 λg)	12-GHz	PB phase	High efficiency, Symmetrical splitting angle.
[51]	CP beam splitting	Micro-fabrication	420nm (0.54 λ_0)	780nm	Propagation phase + PB phase	Rochon-prism-liked, splitting angles independent tuning
[52]	CP beam splitting	PCB	2.07 mm (0.07 λ_0)	10-GHz	Propagation phase + PB phase	Large deflecting angle, Splitting angles independent tuning
This work	CP beam splitting	3-D printing	30.9 mm (4.88 λg)	30-GHz	Propagation phase + QWP	Low cost, splitting angles independent tuning, lens

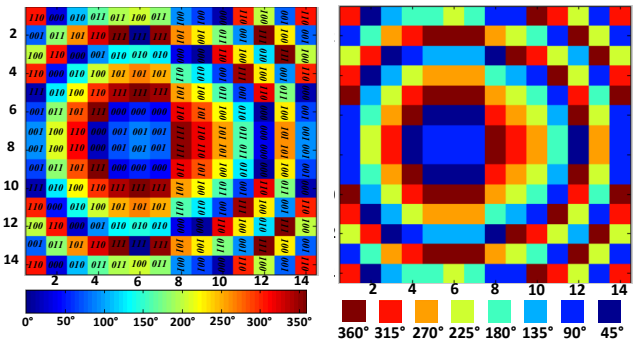

Fig. 18. (a) Compensating phase at the lens aperture and the corresponding code. (b) The discretized phase distribution at the aperture using coding unit cell.

bandwidth. Therefore, lenses that can convert LP to the CP radiation are preferable. By using the low-cost 3-D printing technique, CP-lenses working at 60-GHz [32] and 300-GHz [33] with wide axial ratio bandwidth and high gain were proposed. Both of these CP lenses are realized by stacking a separate circular polarizer to change the polarization with a hemisphere lens or transmit-array atop to collimate the CP beams. By taking advantages of the 3-bit coding polarizer, our design can be regarded as a truly CP lens, which merges two features, namely, the polarization conversion and the beam collimation, together in a single component seamlessly. Therefore, considering the dielectric wavelength (λ_g), the thickness of the proposed lens (30.9 mm, 4.88 λ_g at 30-GHz) is lower than the design in [32] (16.5mm, 5.61 λg at 60-GHz) and [33] (4.2 mm, 6.85 λg at 300-GHz). Compared with other ultrathin thickness transmit-array using PCB technology [45-47], the proposed 3-D printed lens show lower cost and wider AR bandwidth because polarization conversion and phase requirements are not based on resonance.

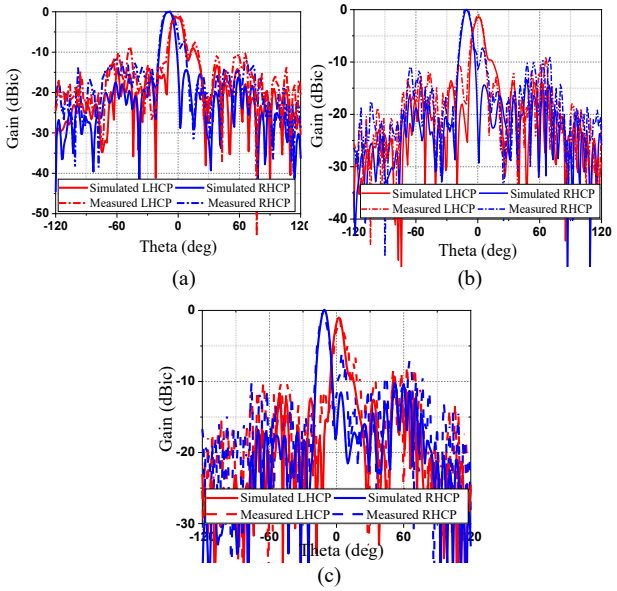

Fig. 19. Simulated and measured radiation patterns of Rochon-prism-like circularly polarized beam shaping lens at (a) 28-GHz (b) 30-GHz and (c) 32-GHz.

Table III compares the proposed circularly polarization beam splitting lens with other relative designs. Anisotropic gradient-index metamaterials can be used to manipulate the orthogonal linearly polarization beams independently with large deflecting angles [5], [48]. As for the circular polarization, using Pancharatnam-Berry (PB) phase to realize the beam splitting is a common approach [49], [50]. However, PB-based beam splitters can only symmetrically split the LHCP and the RHCP beams as the Wollaston prism does for linearly polarized beams. Recently, by combining the propagation phase and PB phase, the design in [51], [52] are capable of independently

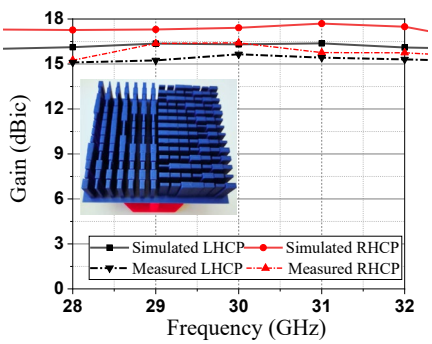

Fig. 20. Simulated and measured peak gain of the Rochon-prism-like circularly polarized beam shaping lens (The inset shows the printed prototype).

manipulating the angles of LHCP/RHCP beams. However, they are unable to collimate the beams. More importantly, since these designs still use PB phase, their beam manipulations are limited to circularly polarizations. Whereas the proposed design can be extended to beam splitting lens with one beam of circular polarization and the other beam with linear polarization.

VI. CONCLUSION

In summary, we have demonstrated planar dielectric linear-to-circular polarization conversion and beam shaping lenses. Different from a conventional polarizer with uniform QWP, the QWP cells used in our design have the same thickness but different length and width. Therefore, they can provide different transmission phase and then can be coded with 3-bit coding. By properly arranging the coding cells, the CP polarization conversion and beam collimation are easily merged together to form new CP-lenses. We demonstrated a CP lens with a boresight pencil-beam, Wollaston-prism-like and Rochon-prism-like planar circularly polarized beam-splitting lenses as examples of the methodological approach.

ACKNOWLEDGEMENT

The authors would like to give their sincere appreciations to Dr. Bin Xi from Sun Yat-Sen University for the help of the antenna measurement. Special thanks to the University of Technology Sydney Tech Lab for funding support, the Blue Sky and Research Academic Program schemes.

REFERENCES

[1] D. Tang, C. Wang C, Z. Zhao, et al. “Ultrabroadband superoscillatory lens composed by plasmonic metasurfaces for subdiffraction light focusing,” *Laser & Photonics Reviews*, 9(6): 713-719, 2015.
[2] Zhang Z, Wen D, Zhang C, et al. Multifunctional light sword meta-surface lens. *ACS photon.*, 5(5): 1794-1799, 2018.
[3] R Rajasekharan, C Bay, Q Dai, J Freeman, TD Wilkinson, Electrically reconfigurable nanophotonic hybrid grating lens array, Applied Physics Letters 96 (23), 233108 (2010)
[4] K Won, A Palani, H Butt, PJW Hands, R Rajeskharan, Q Dai, A. A. Khan, Gehan AJ Amaratunga, Harry J Coles, Timothy D Wilkinson, Electrically Switchable Diffraction Grating Using a Hybrid Liquid Crystal and Carbon Nanotube Based Nanophotonic Device, Advanced Optical Materials 1 (5), 368-373 (2013)
[5] T. Cai et al., "Ultra-Thin polarization beam splitter using 2-D transmissive phase gradient metasurface," *IEEE Trans. Antennas Propag.*, vol. 63, no. 12, pp. 5629-5636, Dec. 2015.
[6] Z. Wei, Y. Cao, X. Su, et al. “Highly efficient beam steering with a transparent metasurface,” *Opt. Exp*, 21(9): 10739-10745, 2013.
[7] Y. Li, X. Li, L. Chen, et al., “Orbital angular momentum multiplexing and demultiplexing by a single metasurface,” *Adv. Opt. Mater.*, 5(2): 1600502. 2017.
[8] S. Yu, L. Li, G. Shi, et al., “Generating multiple orbital angular momentum vortex beams using a metasurface in radio frequency domain,” *Appl. Phys. Lett.*, 108(24): 241901,2016.
[9] C. Zhang, L. Deng, J. Zhu, et al. “Control of the spin angular momentum and orbital angular momentum of a reflected wave by multifunctional graphene metasurfaces,”. *Materials,* 11(7): 1054. 2018.
[10] S.O. Kasap, R.K. Sinha, Optoelectronics and photonics: principles and practices. New Jersey: Prentice Hall, 2001.
[11] A. Saha, K. Bhattacharya, and A. K. Chakraborty, “Achromatic quarter-wave plate using crystalline quartz,” *Appl. Opt.* 51, 1976–1980, 2012.
[12] J. B. Masson and G. Gallot, “Terahertz achromatic quarter-wave plate,” *Opt. Lett.* 31, 265–267. 2006.
[13] P. Weis, O. Paul, C. Imhof, R. Beigang, M. Rahm, "Strongly birefringent metamaterials as negative index terahertz wave plates", *Appl. Phys. Lett.,* vol. 95, no. 17, Oct. 2009.
[14] M. Joyal and J.-J. Laurin, “Analysis and design of thin circular polarizers based on meander lines,” *IEEE Trans. Antennas Propag.*, vol. 60, no. 6, pp. 3007–3011, Jun. 2012.
[15] L. Young, L. Robinson and C. Hacking, "Meander-line polarizer," *IEEE Trans. Antennas Propag*, vol. 21, no. 3, pp. 376-378, May 1973.
[16] P. Fei, Z. Shen, X. Wen, et al. “A single-layer circular polarizer based on hybrid meander line and loop configuration,” *IEEE Trans. Antennas Propag*, , 63(10): 4609-4614, 2015.
[17] J. Yin, X. Wan, J. Ren, et al., “A circular polarizer with beamforming feature based on frequency selective surfaces,”. *Sci. Rep.*, 7: 41505, 2017.
[18] M. Akbari, M. Farahani, A. Sebak and T. A. Denidni, "Ka-Band Linear to Circular Polarization Converter Based on Multilayer Slab With Broadband Performance," *IEEE Access,* vol. 5, pp. 17927-17937, 2017.
[19] J. Wang, Z. Shen, W. Wu, and K. Feng, “Wideband circular polarizer based on dielectric gratings with periodic parallel strips,” *Opt. Exp.*, vol. 23, no. 10, pp. 12533–12543, May 2015.
[20] K. X. Wang and H. Wong, "A wideband millimeter-wave circularly polarized antenna with 3-D printed polarizer," *IEEE Trans. Antennas Propag*, vol. 65, no. 3, pp. 1038-1046, March 2017.
[21] H. Jiang, W. Zhao, and Y. Jiang, “All-dielectric circular polarizer with nearly unit transmission efficiency based on cascaded tensor huygens surface,” *Opt. Exp.*, vol. 24, no. 16, pp. 17738–17745, Aug. 2016.
[22] T. S. Rappaport et al., "Millimeter wave mobile communications for 5G cellular: It will work!," *IEEE Access*, vol. 1, pp. 335-349, 2013.
[23] Nasimuddin, X. Qing and Z. N. Chen, "Compact circularly polarized symmetric-slit microstrip antennas," *IEEE Antennas and Propagation Magazine*, vol. 53, no. 4, pp. 63-75, Aug. 2011.
[24] S. Gao, Q. Luo, and F. Zhu, Circularly Polarized Antennas. Hoboken, NJ, USA: Wiley, Nov. 2013.
[25] C. Ding and K. Luk, "A Wideband High-Gain Circularly-Polarized Antenna Using Artificial Anisotropic Polarizer," IEEE Trans. Antennas Propag. vol. 67, no. 10, pp. 6645-6649, Oct. 2019.
[26] M. F. Farooqui and A. Shamim, “3-D inkjet-printed helical antenna with integrated lens,” *IEEE Antennas Wireless Propag. Lett.*, vol. 16, no. 8, pp. 800–803, Aug. 2016.
[27] L. Xue and V. Fusco, “Polarisation insensitive planar dielectric slab waveguide extended hemi-elliptical lens,” *IET Microw., Antennas Propag.*, vol. 2, no. 4, pp. 312–315, Jun. 2008.
[28] Z. Shi, S. Yang, S.-W. Qu, and Y. Chen, “Circularly polarised planar Luneberg lens antenna for mm-Wave wireless communication,” *Electron. Lett.*, vol. 52, no. 15, pp. 1281–1282, 2016.
[29] X. Wu, G.V. Eleftheriades, T.E. van Deventer-Perkins. “Design and characterization of single-and multiple-beam mm-wave circularly polarized substrate lens antennas for wireless communications,” *IEEE Transactions on Micro. Theory. Tech.*, 49(3): 431-441, 2001.
[30] Campo M A, Blanco D, Carluccio G, et al. Circularly polarized lens antenna for Tbps wireless communications[C], 2018 48th European Microwave Conference (EuMC). IEEE, 2018: 1147-1150.
[31] K. X. Wang and H. Wong, "A Wideband Millimeter-Wave Circularly Polarized Antenna With 3-D Printed Polarizer," *IEEE Trans. Antennas Propag*, vol. 65, no. 3, pp. 1038-1046, March 2017.
[32] K. X. Wang and H. Wong, "Design of a wideband circularly polarized millimeter-wave antenna with an extended hemispherical lens," *IEEE Trans. Antennas Propag*, vol. 66, no. 8, pp. 4303-4308, Aug. 2018.

[33] G. Wu, Y. S. Zeng, K. F. Chan, S. Qu and C. H. Chan, "High-gain circularly polarized lens antenna for terahertz applications," *IEEE Antennas Wireless Propag. Lett.* Early access.
[34] C. Pfeiffer, A. Grbic, "Planar lens antennas of subwavelength thickness: Collimating leaky-waves with metasurfaces," *IEEE Trans. Antennas Propag,* 2015, 63(7): 3248-3253.
[35] M. Jiang, Z. Chen, Y. Zhang, et al. "Metamaterial-based thin planar lens antenna for spatial beamforming and multibeam massive MIMO," *IEEE Trans. Antennas Propag*, 65(2): 464-472 2017.
[36] Q. Cheng, H. Ma, T. Cui, "Broadband planar Luneburg lens based on complementary metamaterials,". *Appl. Phys. Lett*, 95(18): 181901 2009.
[37] H. Li, G. Wang, H. Xu, et al. "X-band phase-gradient metasurface for high-gain lens antenna application," *IEEE Trans. Antennas Propag*, 63(11): 5144-5149 2015.
[38] T.J. Cui, Microwave metamaterials. *National Science Review*, 5(2): 134-136. 2017.
[39] T.J. Cui, M.Q. Qi, X. Wan, J. Zhao,and Q. Cheng,"Coding metamaterials, digital metamaterials and programmable metamaterials," *Light, Sci. Appl.*, vol. 3, Art. no. e218 2014.
[40] S. Liu, T.J. Cui, Q. Xu, et al. "Anisotropic coding metamaterials and their powerful manipulation of differently polarized terahertz waves,". *Light, Sci. Appl.* , 5(5): e16076. 2016.
[41] Zhang K, Li D, Chang K, et al. Electromagnetic theory for microwaves and optoelectronics[M]. Berlin: Springer, 1998.
[42] P. Nayeri, F. Yang, and A.Z. Elsherbeni. Reflectarray antennas: theory, designs, and applications. John Wiley & Sons, 2018.
[43] Montarou C C, Gaylord T K. "Analysis and design of modified Wollaston prisms," *Applied optics*, 1999, 38(31): 6604-6616.
[44] Z. Li, et al. "Graphene Plasmonic Metasurfaces to Steer Infrared Light". *Sci. Rep.* 5, 12423; doi: 10.1038/srep12423, 2015.
[45] L. Di Palma, A. Clemente, L. Dussopt, R. Sauleau, P. Potier and P. Pouliguen, "Circularly Polarized Transmitarray With Sequential Rotation in Ka-Band," *IEEE Trans. Antennas Propag*, vol. 63, no. 11, pp. 5118-5124, Nov. 2015.
[46] Yu J, Chen L, Shi X. "A multilayer dipole-type element for circularly polarized transmitarray applications," *IEEE Antennas Wireless Propag. Lett*, 2016, 15: 1877-1880.
[47] C. Tian, Y. Jiao and G. Zhao, "Circularly Polarized Transmitarray Antenna Using Low-Profile Dual-Linearly Polarized Elements," *IEEE Antennas Wireless Propag. Lett*, vol. 16, pp. 465-468, 2017.
[48] H. F. Ma, G. Z. Wang, W. X. Jiang, and T. J. Cui, "Independent control of differently-polarized waves using anisotropic gradient-index metamaterials," *Sci. Rep.*, vol. 4, p. 6337, 2014.
[49] W. Luo, S. Xiao, Q. He, S. Sun, L. Zhou, "Photonic Spin Hall Effect with Nearly 100% Efficiency," *Adv. Opt. Mater.* 3, 1102− 1108, 2015.
[50] C. Liu et al. "Fully controllable pancharatnam-berry metasurface array with high conversion efficiency and broad bandwidth. *Sci. Rep.* 6, 34819; doi: 10.1038/srep34819 2016.
[51] B. Wang, F. Dong, H. Feng, et al. "Rochon-Prism-like planar circularly polarized beam splitters based on dielectric metasurfaces,". *ACS Photon*.5, 1660 − 1664 , 2017.
[52] Y. Yuan, K. Zhang, X. M. Ding, B. Ratni, S. N. Burokur, Q. Wu, "Complementary transmissive ultra-thin meta-deflectors for broadband polarization-independent refractions in the microwave region", *Photon. Res.*, vol. 7, no. 1, pp. 80-88, 2019.